A Fast Optical Propagation Technique
for Modeling Micro-Optical Systems

Timothy P. Kurzweg[*], Steven P. Levitan[*], Jose A. Martinez[*], Mark Kahrs[*], Donald M. Chiarulli[+]

[*]University of Pittsburgh, Department of Electrical Engineering, Pittsburgh, PA, USA,

tim@ee.pitt.edu, steve@ee.pitt.edu, jmarti@ee.pitt.edu, kahrs@ee.pitt.edu

[+]University of Pittsburgh, Department of Computer Science, Pittsburgh, PA, USA, don@cs.pitt.edu

ABSTRACT

As designers become more aggressive in introducing optical components to micro-systems, rigorous optical models are required for system-level simulation tools. Common optical modeling techniques and approximations are not valid for most optical micro-systems, and those techniques that provide accurate simulation are computationally slow. In this paper, we introduce an angular frequency optical propagation technique that greatly reduces computation time while achieving the accuracy of a full scalar formulation. We present simulations of a diffractive optical MEM Grating Light Valve to show the advantages of this optical propagation method and the integration of the technique into a system-level multi-domain CAD tool.

Categories and Subject Descriptors

I.6.5 [**Simulation and Modeling**]: Model Development - *modeling methodologies*

General Terms

Algorithms, Design

Keywords

Optical Propagation, Angular Spectrum, CAD, Optical Micro-systems, Optical MEMS

1. INTRODUCTION

It is well known that optics can provide advantages to micro-systems in terms of speed, bandwidth and reduced power [12]. However, by adding this optical domain to micro-systems, many new challenges are introduced in system design. In these multi-domain systems, optical effects, such as diffraction, interference, and scattering, are critical to the success or failure of the designs. Therefore, optical modeling and simulation are crucial in the design stage of the micro-system.

Currently, multi-domain micro-systems are simulated by point-tools using component level models performed at the physical level. These tools are typically domain specific and computationally complex. In contrast, system-level

tools are designed to include multiple domains and allow efficient system simulation, by modeling components by their functionality rather than their physical construction. Established MEM (micro-electrical-mechanical) system-level modeling tools exist, with physical device models being extracted into behavioral-level models. However, optical propagation models are not easily integrated into these existing tools.

When optical wavefronts interact with the small feature sizes of micro-systems, many of the common optical propagation modeling techniques become invalid, and full vector or scalar solutions to Maxwell's equations are required for accurate simulation [7]. However, these accurate solutions are computationally intensive, making interactive design between system designer and CAD tool almost impossible. As more optical components are introduced into micro-systems and the systems become more complex, the demand for computationally efficient simulation tools increases. Therefore, the problem of optical modeling in MOEM (micro-electro-opto-mechanical) systems is two-fold: first, a rigorous model is needed to model optical propagation, and, second, the model must be computationally efficient.

In this paper, we present a solution for both parts of the problem. We introduce an optical propagation model that provides valid results in the micro-system domain, with a computational algorithm that allows for interactive CAD design. We first provide motivation for modeling tools for MOEM systems and components by examining a Grating Light Valve device (GLV). This is followed by a brief background of optical propagation modeling, from which we determine a valid scalar technique for optical MEM system modeling. Next, a description of the angular spectrum technique, which we use to reduce the computational load, is provided. System-level simulations and analyses of a GLV system follow. We conclude with a summary and discussion of future work.

2. MOTIVATION

To provide motivation for our work, we first examine one of the more promising MOEM components, the Grating Light Valve [1]. This device has many display applications, including digital projection, HDTV, and vehicle displays. The GLV is simply a MEM (micro-
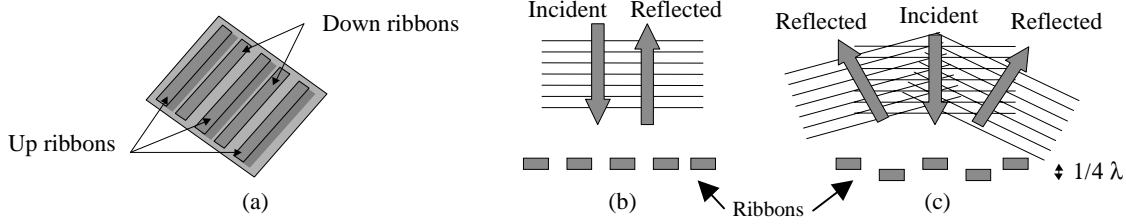
Figure 1: GLV Device (a) Top View and Side View Operation for (b) Up Ribbons and (c) Down Ribbons

electrical-mechanical) phase grating made from parallel rows of reflective ribbons. When all the ribbons are in the same plane, incident light that strikes normal to the surface reflects 180 degrees off the GLV. However, if alternating ribbons are moved down a quarter of a wavelength, a "square-well" diffraction pattern is created, and the light is reflected at an angle from that of the incident light. The angle of reflection depends on the width of the ribbons and the wavelength of the incident light. Figure 1 shows the ribbons, from both a top and side view, and also the reflection patterns for both positions of the ribbons.

The GLV component is fabricated using standard silicon VLSI technology, with ribbon dimensions approximately 3-5µm wide and 20-100 µm long [1]. Each ribbon moves through electro-static attraction between the ribbon and an electrode fabricated underneath the ribbon. This electro-static attraction moves the ribbons only a few hundred nanometers, resulting in an approximate switching time of 20 nsec. Since the GLV depends on a diffractive phenomenon to direct the light beam, a rigorous modeling technique is required for modeling the GLV system.

3. OPTICAL PROPAGATION

Optical propagation can be modeled completely by the solution of Maxwell's equations for both the electric field vector, $\vec{E}$, and the magnetic field vector, $\vec{H}$ [4]. Solutions for these fields are typically done with a Beam Propagation Method (BPM), using a Fourier Transform, or a finite-difference time-domain (FDTD) algorithm. This vector method is valid for optical propagation in micro-systems, however, the computation time and memory requirements are extremely demanding.

To reduce the computational resources of the vector solutions, a scalar representation is commonly used. Scalar optics are defined by summarizing vectors $\vec{E}$ and $\vec{H}$ by a single complex scalar, U. This replacement is valid if the propagation medium is dielectric, isotropic, homogenous, nondispersive, and nonmagnetic. Propagation through free-space meets these requirements. No longer are we solving in 3D, as the scalar function represents a complex 2D wave function.

This complex scalar must satisfy the Helmholtz wave equation, $(\nabla^2 + k^2)U = 0$, where, the wave number, $k=2\pi/\lambda$. With use of Green's theorem, the Rayleigh-Sommerfeld formulation is derived from the wave equation for the propagation of light in free-space [4]:

$$U(x, y, z) = \frac{z}{j\lambda} \iint_\Sigma U(\xi, \eta, 0) \frac{\exp(jkr)}{r^2} \partial\xi\partial\eta$$

where, $r = \sqrt{z^2 + (x-\xi)^2 + (y-\eta)^2}$, Σ is the area of the aperture, and z is the distance that the light is propagated from an aperture plane ($z = 0$) to an observation plane. It is assumed that the two planes are parallel, with coordinate systems $(\xi,\eta,0)$ in the aperture plane and (x,y,z) in the observation plane, as seen in Figure 2. The formulation is valid as long as both the propagation distance and the aperture size are greater than the wavelength of light. These restrictions are based on the boundary conditions of the Rayleigh-Sommerfeld formulation, and the fact that the electric and magnetic fields cannot be treated independently at the boundaries of the aperture [4].

To compute the complex wave front at the observation plane, we divide both the aperture plane and the observation plane into gridded meshes, as seen in Figure 2. Both planes are commonly meshed into NxN regions, where N is the number of mesh points along the side of a square. Using a direct integration technique we have successfully shown results using the Rayleigh-Sommerfeld method [7]. However, this direct integration method is computationally intensive, with a computational order of O(N^4).

The far (Franhofer) and near (Fresnel) field approximations of the scalar formulation reduce the computational intensity, using a FFT for optical propagation. However, we have previously shown that these techniques are not valid for typical micro-system dimensions [7]. We have also shown that efficient Gaussian beam propagation
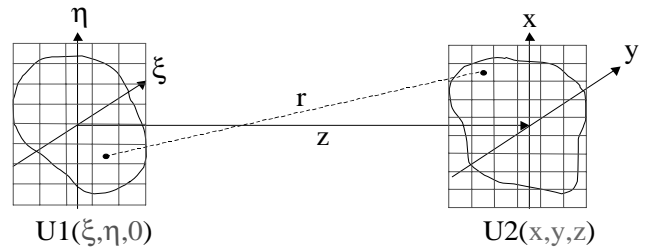

Figure 2: Aperture and Observation Coordinate System in the Rayleigh-Sommerfeld Approximation

techniques have limitations for optical MEM simulation. In the interest of reducing the computational load of using a full scalar technique, we look to recast the full Rayleigh-Sommerfeld formulation using the angular spectrum technique.

4. ANGULAR SPECTRUM TECHNIQUE

As an alternative to direct integration over the surface of the wavefront, the Rayleigh-Sommerfeld formulation can also be solved using a technique that is similar to solving linear, space invariant systems. In this case, the complex wavefront is analyzed across its surface with a Fourier transform. By using the Fourier transform, the complex optical wavefront is reduced into a set of simple linear exponential functions. This transform identifies the components of the angular spectrum, which are plane waves traveling in different directions away from the surface [4].

Examining the angular spectrum, we look at light propagating from an aperture plane at z=0 to a parallel observation plane. The wave function U(x,y,0) has a 2D Fourier transform, $A(v_x,v_y,0)$, in terms of angular frequencies, v_x and v_y.

$$A(v_x, v_y, 0) = \iint U(x, y, 0) \exp[-j2\pi(v_x x + v_y y)] \, \partial x \partial y$$

where, $v_x = \sin \theta_x / \lambda$ and $v_y = \sin \theta_y / \lambda$.

$\sin(\theta_x)$ and $\sin(\theta_y)$ are the directional cosines of the plane wave propagating from the origin of the coordinate system, as seen in Figure 3. A is the complex amplitude of the plane wave decomposition defined by the specific angular frequencies.

To propagate the complex wave function to a parallel plane, a propagation phase term is used as a transfer function. The relationship of propagation in the frequency domain between $A(v_x,v_y,0)$ and $A(v_x,v_y,z)$ has been computed by satisfying the Helmhotz equation with the propagated complex wave function, U(x,y,z) [4]:

$$A(v_x, v_y, z) = A(v_x, v_y, 0) \exp\left\{ jz2\pi\sqrt{\frac{1}{\lambda^2} - v_x^2 - v_y^2} \right\}$$
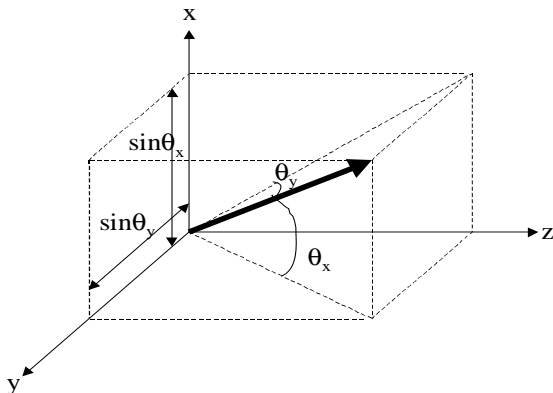

Figure 3: Angular Spectrum Frequencies

This describes the phase difference that each of the plane waves, differentiated by the angular, or spatial, frequencies, experiences due to the propagation between the parallel planes. Therefore, the wave function after propagation can be transformed back into the spatial domain with the following inverse Fourier transform:

$$U(x, y, z) = \iint A(v_x, v_y, 0) \exp\left\{ jz2\pi\sqrt{\frac{1}{\lambda^2} - v_x^2 - v_y^2} \right\} \times$$
$$\exp[j2\pi(v_x x + v_y y)] \, \partial v_x \partial v_y$$

It is interesting to note that the output complex wavefunction is simply the convolution of the input wave function and the propagation phase function. Using Fourier transform theory, the convolution in the spatial domain is performed by a multiplication in the frequency domain.

It is appropriate to discuss the physical effect of evanescent waves, which are defined in the case when, $1/\lambda^2 - v_x^2 - v_y^2 < 0$. These waves carry very little power and die out in a couple of wavelengths of propagation [6]. In our simulations, we ignore these waves.

The angular spectrum method is restricted to propagation between parallel planes that share a common center. Removing these restrictions has been the goal of recent research. Tommoasi and Bianco have determined how to propagate to a plane that is tilted with respect to initial plane [10]. Delen and Hooker have determined a way to allow offsets in the observation plane [3]. We summarize these two methods next.

For arbitrary angles between the aperture plane, U(ξ,η,ζ) and the observation plane, U(x,y,z), a mapping of the spatial frequencies in each plane's coordinates system must occur. This mapping is possible due to the fact that the phase accumulation term does not change when the waves propagate to an observation plane that is not normal to the aperture plane. It can be found that the rotational matrix, M, relating (ξ,η,ζ) to (x,y,z), can be used to relate spatial frequencies in the two coordinate systems by [10]:

$$(x, y, z)^t = M(\xi, \eta, \zeta)^t \qquad (v_\xi, v_\eta, v_\zeta)^t = M^t (v_x, v_y, v_z)^t$$

In the new tilted coordinate system, the incoming spatial frequencies are perceived as having spatial frequency corresponding to the outgoing coordinate system. For example, the incoming aperture plane wave having spatial frequencies (0,0) correspond to angle (-ϕ,0) in the observation plane with a ϕ tilt in the y-direction. In all cases, even if the spatial frequencies are re-mapped, the amplitude of the plane wave remains constant.

For an observation plane whose center is offset from the propagation axis of the aperture plane, the Fourier shifting theorem can be used to solve for the complex wave function [3]. With this relation between the offset of the coordinate systems, the function for free-space propagation between offset planes is:

$$U(x,y,0) = \iint A'(v_x, v_y, 0) \exp\left\{ jz2\pi\sqrt{\frac{1}{\lambda^2} - v_x^2 - v_y^2} \right\} \times$$

$$\exp[j2\pi(v_x x + v_y y)]\, \partial v_x \partial v_y$$

where,

$$A'(v_X, v_Y, 0) = A(v_X, v_Y, 0) \exp[j2\pi(v_x(x'-x) - v_y(y'-y)]$$

The advantage of using the angular spectrum to model light propagation is that the method is based on Fourier transforms. In CAD tools, the Fourier transform can be implemented by one of the numerous Fast Fourier Transform (FFT) techniques. The computational order of the FFT for a 2D input, is $O(N^2 \log_2 N)$, obviously more efficient when compared to the direct integration method. We show this speed increase later through example.

In continuous theory, the angular spectrum method is an exact solution of the Rayleigh-Sommerfeld formulation. However, when solving the algorithm on a digital computer, a Discrete Fourier Transform (DFT) must be used, resulting in the accuracy of the angular spectrum method depending on the resolution, or spacing, of the aperture and observation plane meshing. We call the physical size of the aperture and observation planes the "bounding box", defining the size of the optical wavefront being propagated. Since the complex wave function is only non-zero for a finite space in the bounding box, the signal is not always bandwidth limited, and the Nyquist sampling theory does not always apply. It can be shown, however, that the resolution of the aperture and observation meshing must be $\lambda/2$ or smaller [3]. For many simulation systems without large degrees of tilt and hard diffractive apertures, the resolution can be coarser. In systems with high tilts, the resolution is most sensitive. With a mesh spacing of $\lambda/2$, the angular spectrum decomposition will ensure plane waves propagating from aperture to observation plane in a complete half circle, that is, between –90 and +90 degrees.

Other inaccuracies that can occur when using a discrete Fourier transform are aliasing and window truncation. Aliasing occurs when frequencies exist greater than the critical sampling frequency. In this case, these high frequencies are "folded over" into the sampled frequency range [2]. The effect of this is seen in our simulations as optical power "reflecting" off of the walls of the bounding box. If significant optical power reflects off the wall, interference between the propagating beam and these reflections can occur, resulting in inaccurate optical waveforms. The same effect can be seen when the bounding box truncates the signal. Truncation occurs when the waveform propagates into the edges of the bounding box. The simplest solution toward accurate results is having sufficient zero padding around the optical waveform, reducing the chance the waveform is aliased or truncated off the walls of the bounding box.

This work has been implemented in our system-level, multi-domain CAD tool, Chatoyant [7]. Chatoyant supports modeling and simulation in the optical, electrical, and mechanical domains. The electrical and mechanical simulations are implemented using a piece-wise linear Modified Nodal Analysis technique [8]. The optical simulation supports both Gaussian propagation and the angular spectrum technique presented in this paper.

5. GLV SIMULATIONS

The advantages of the angular spectrum method are best seen through example. We simulate and analyze the GLV system, as presented earlier, in Chatoyant. For the simulation of the GLV, we examine one optical pixel. A projected pixel is diffracted from a GLV composed of 4 ribbons, two stationary and two that are movable [1]. Each ribbon has a length of 20 μm and a width of 5 μm. Ideally, there is no gap between the ribbons, however, in reality, a gap is present and is a function of the feature size of the fabrication. Although this gap can be modeled in our tool, in these simulations, we provide an ideal GLV simulation with no gap.

The GLV is modeled as a phase grating, where the light that strikes the down ribbons propagates a half of a wavelength more than the light that strikes the up ribbons. In our model, light reflecting from the down ribbons is multiplied by a phase term. The phase term is similar to a propagation term through a medium: $U_{down\_ribbon} = U\exp(j2kd)$, where, d is the distance that the ribbon is moved towards the substrate, typically $\lambda/4$ for the GLV.

Far-field diffraction theory states the diffracted angle reflected from the square-well grating is [5]: $\theta = q\lambda/a$, where, q is the diffraction mode $(0, \pm1, \pm2, \pm3,\ldots)$, a is the period of the diffractive grating, and θ is in radians. In the special case of a square well, when light is diffracted by a grating with a displacement of $\lambda/4$ (a $\lambda/2$ optical path difference after reflection), all the optical power is diffracted from the even modes into the odd modes [9].

In the first simulation, the standard operation of the GLV is verified. We assume an incident plane wave of green light (λ=520 nm) striking the grating, with the square-well period defined by the ribbon width, and no gap. We simulate the GLV in both cases, that is, when all the ribbons are on the same plane and when the alternating ribbons are moved downward a distance of $\lambda/4$. In this example, the light is reflected off of the grating and propagated 1000 μm to an observation plane. A bounding box of 400x400 μm is used, with N equal to 2048. Intensity contours of the observation plane are presented in Figure 4(a and b).

When the grating is moved into the down position, all of the optical power is not transferred into the expected odd far-field diffractive modes. This is seen in the center of Figure 4(b), as small intensity clusters are scattered between the $\pm1^{st}$ modes. This scattering is a near field
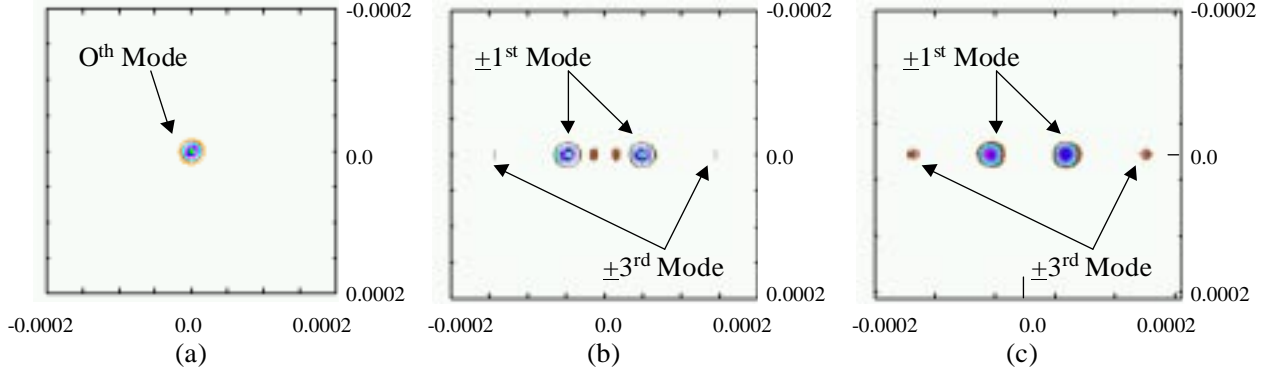
Figure 4: GLV Operation (a) All Ribbons Up (b) Alternating Ribbons Down (c) Fraunhofer Approximation

effect, and demonstrates that in this system, light propagating 1000 μm is not in the far-field. If a designer used a tool propagating with the Fraunhofer far-field approximations, these scattering effects would not be detected. For example, when running the same simulation on LightPipes [11], a CAD tool using the Fraunhofer approximation for optical propagation, only the far-field pattern of light diffracted into the 1st and 3rd modes is seen, as presented in Figure 4(c). When comparing this result to Figure 4(b), it is shown that far field approximation is not valid for this propagation distance. Through this example we have shown that using the angular frequency technique, we achieve the full Rayleigh-Sommerfeld accuracy, while obtaining the same computational speed of using the Fraunhofer approximation.

To show the advantage of the angular spectrum method, we compare the run time of the above simulation with the run time using the direct integration method. With N=2048, the FFT simulation takes about 1.5 minutes. The direct integration technique takes approximately 5.5 days to finish. If N is reduced to 1024, the simulation completes in approximately 25 seconds, whereas the direct integration simulation takes approximately 32 hours. These simulations were run on a 1.7 GHz dual-processor PC running Linux, with 2 GB of main memory.

In the next simulation, we perform a transient sweep of the ribbon movement, from 0 to 150 nm. The rest of the
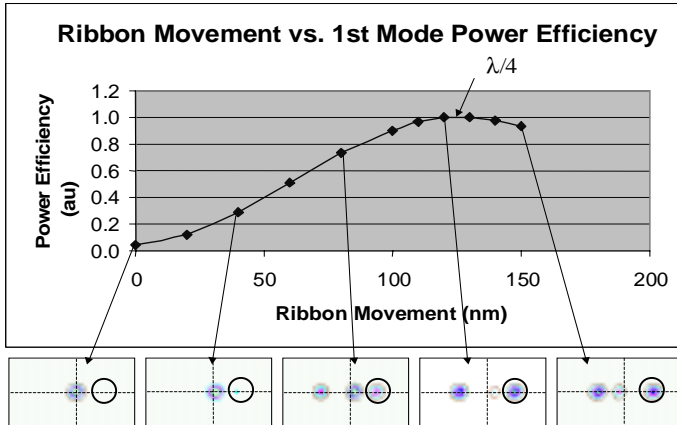
system setup is exactly the same as before. However, this time, we simulate the normalized power efficiency captured in the 1st diffraction mode for different ribbon depths. To simulate this, a circular detector (radius=12.5μm) is placed on the positive 1st mode. Figure 5 is a graph that shows the simulated normalized power efficiency in this first mode. As the ribbons are moved downward, more optical power is diffracted into the non-zero modes. As the ribbons reach the λ/4 point, almost all the diffractive power is in the $\pm 1^{st}$ mode. Figure 5 also includes intensity contours of selected wavefronts during the transient simulation, along with markings of the system origin and circular detector position. From these wavefronts, interesting diffractive effects can be noted. As expected, when there is little or no ribbon movement, all the light is in the 0th mode. However, with a little ribbon movement, it is interesting to note that the 0th mode is "steered" at a slight angle from the origin. As the ribbons move downward about λ/8, the energy in the $\pm 1^{st}$ modes are clearly defined. As the gratings move closer to the λ/4 point, the power is shifted from the 0th mode into the $\pm 1^{st}$ modes, until there is a complete switch. As the ribbons move past the λ/4 point, optical power shifts back into the 0th mode.

In the final simulation, we present a full system-level example as we expand the system to show a complete end-to-end link used in a configuration of a color projection system. The system is shown in Figure 6. In this system, we model light, passing through a color wheel, striking a prism, reflecting off the GLV device, past a screen, focused by a lens, and striking a detector [1]. In this system, when the GLV ribbons are all up, the screen blocks the light's 0th mode and the pixel is not displayed. When the alternating

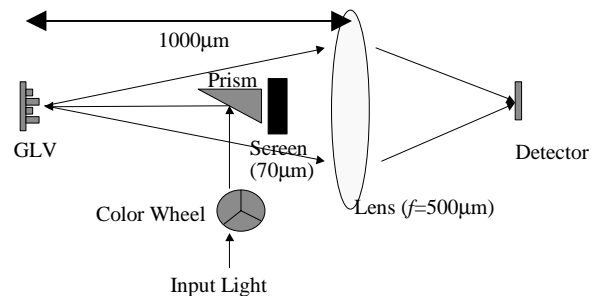**Figure 5: Transient Analysis of Ribbon Movement and Intensity Contours**

Figure 6: End-to-end GLV Display Link

ribbons are pulled down, the lens focuses the light found in the $\pm 1^{st}$ modes and converges them to the center of the system, displaying the pixel. Using a spinning color wheel to change the wavelength of the incident light, a frame-sequential GLV projection system uses red (680 nm), green (530 nm), and blue (470 nm) light on the same grating [1]. Since the same grating is used for all wavelengths of light, the grating movement is tuned for the middle frequency: 130 nm (λ_{green}/4). During this simulation, we use a hybrid approach for the optical modeling. For the propagation through the color wheel and the prism, we use Gaussian propagation. Since propagating through these components does not diffract the beam, this Gaussian technique is not only efficient, but valid. However, as soon as the light propagates past the prism component, we switch the optical propagation technique to our full scalar method to accurately model the diffraction off of the GLV device. The remainder of the simulation is propagated with the scalar technique.

We analyze the system by looking at the amount of optical power that is being received on a centered circular detector (radius 10μm) for the different wavelengths of light, since we are using the same GLV that is tuned for the green wavelength for all wavelengths. A sweep of the distance between the focusing lens and the detector plane is simulated for 0 to 1500 μm, when the GLV ribbons are pulled down. The graph in Figure 7 shows the normalized power received on the circular detector for each wavelength along with selected intensity contours of the green wavefront as the beam propagates past the lens. For clarity, the detector's size and position is added onto the intensity contours. For distances under 600 μm, the light remains in its two positive and negative 1st modes, as the convergence of the beams has not occurred, resulting in zero power being received on the center detector. As expected, each of the wavelengths focuses at a different rate, as shown by each the wavelength's specific curve in Figure 7. However, it is seen that all wavelengths focus and achieve detected
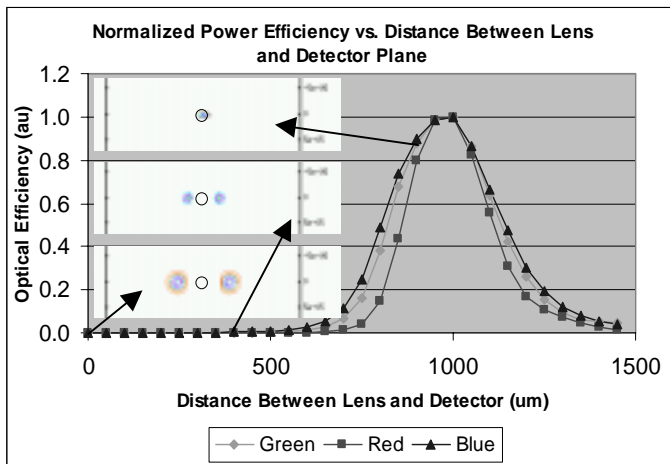
maximum power at a distance past the lens of 1000 μm, or twice the lens' focal length. At this point, all three colors project on top of each other, creating a color pixel in the focal plane. With additional optics, this focal plane can be projected to a screen outside the projector. This simulation has shown that the grating, although tuned for the green wavelength, can be used for all three wavelengths.

6. SUMMARY

In this paper, we have demonstrated a promising optical propagation technique that can greatly speed-up simulation of optical micro-systems. We have shown how to achieve full scalar diffraction with the use of a FFT, by using the angular spectrum of light. This reduces an $O(N^4)$ direct integration problem to $O(N^2\log N)$. With the angular spectrum method, we can achieve the speed of the Fraunhofer technique, without any of the required approximations of using that technique. We have used the GLV as a typical micro-system to motivate our work, and presented full system-level simulation results of this device. In future work, we plan to extend the angular spectrum technique to support roughness and non-planar surfaces.

7. REFERENCES

[1] Bloom, D.M., "The Grating Light Valve: Revolutionizing Display Technology," Photonics West, Projection Displays III, 1997.

[2] Briggs, W.L. and Henson, V.E., The DFT: An Owner's Manual for the Discrete Fourier Transform, (SIAM, 1995).

[3] Delen, N., Hooker, B., "Free-space Beam Propagation Between Arbitrarily Oriented Planes Based on Full Diffraction Theory: a Fast Fourier Transform Approach," JOSA, Vol. 15, No. 4, April 1998, pp. 857-867.

[4] Goodman, J.W., Introduction to Fourier Optics, Second Edition (The McGraw-Hill Companies, Inc., 1996).

[5] Hecht, E., Optics, Second Edition (Addison-Wesley Publishing Company, 1987).

[6] Kowarz, M.W., "Diffraction Effects in the Near Field," Ph.D. Thesis, University of Rochester, NY, 1995.

[7] Kurzweg, T.P., Levitan, S.P., Martinez, J.A., Marchand, P.J., Chiarulli, D.M., "Diffractive Optical Propagation Techniques for a Mixed-Signal CAD Tool," Optics in Computing (OC2000), Quebec City, CA, June 18-23, 2000.

[8] Martinez, J.A., Kurzweg, T.P., Levitan, S.P., Marchand, P.J., Chiarulli, D.M., "Mixed-Technology System-Level Simulation", Analog Integrated Circuits and Signal Processing, Vol. 29, pp. 127-149, October/November 2001.

[9] Solgaard, O., "Integrated Semiconductor Light Modulators for Fiber-Optic and Display Applications," Ph.D. Thesis, Stanford University, 1992.

[10] Tommasi, T., Bianco, B., "Frequency Analysis of Light Diffraction Between Rotated Planes," Optics Letters, Vol. 17, No. 8, April 1992, pp.556-558.

[11] Vdovin, G., LightPipes Manual, http://guernsey.et.tudelft.nl

[12] Wu, M.C., "Micromachining for optical and Optoelectronic Systems," Proceedings of the IEEE, Vol. 85, No. 11, November 1997, pp. 1833-1856.

Figure 7: Wavelength Power vs. Distance Propagated